Acta Materialia 101 (2015) 48–54

Contents lists available at ScienceDirect

Acta Materialia

journal homepage: www.elsevier.com/locate/actamat

Twin-like defects in $L1_0$ ordered τ-MnAl-C studied by EBSD

F. Bittner [a,b,*], L. Schultz [a,b], T.G. Woodcock [a]

[a] IFW Dresden, Institute for Metallic Materials, PO Box 270116, 01171 Dresden, Germany
[b] TU Dresden, Institute of Materials Science, 01062 Dresden, Germany

ARTICLE INFO

Article history:
Received 17 June 2015
Accepted 19 August 2015
Available online 21 September 2015

Keywords:
Electron backscattered diffraction (EBSD)
Grain boundary structure
Hard magnetic material
Rare earth free
Coercivity

ABSTRACT

Twin-like defects in τ-MnAl-C, which has the $L1_0$ structure, have been studied using electron backscattered diffraction (EBSD) in as-transformed and in subsequently hot extruded samples. In both states, three distinct twin-like defects were found, whose misorientations were described by rotations of 62°, 118° and 180° about the normal to {1 1 1}. These are denoted as pseudo twins, order twins and true twins, respectively. The true twins are often observed in this type of material. The order twins formed the boundaries between regions where the *c*-axes were almost perpendicular to each other and these were thought to form due to the accumulation of strains during the transformation to τ from the hexagonal parent phase, ε. Due to symmetry, pseudo twins necessarily appeared at points where order twins interacted with true twins. The frequency of the different defects was very sensitive to the sample state. As the parent phase ε is not involved in the dynamic recrystallization which occurred during hot extrusion, there was a greatly reduced fraction of order twins and pseudo twins in the hot extruded state. The misorientation angle of the magnetically easy ⟨0 0 1⟩ axis across the three twin-like defects was 48°, 86° and 75° for pseudo, order and true twins, respectively. The interaction of the three twin-like defects with 180° magnetic domain walls and the resulting effect on the magnetic properties of the material may therefore be different.

1. Introduction

The ferromagnetic $L1_0$ phase (P4/mmm, AuCu I type) in the Mn–Al system, known as τ, has intrinsic magnetic properties (anisotropy constant $K_1 > 1$ MJ/m^3 [1], saturation magnetisation $\mu_0 M_s > 0.7$ T [1,2] and Curie temperature $T_c > 300$ °C [1,3]), which make it highly interesting as a possible rare earth free permanent magnet with an energy density between those of ferrites and rare earth based magnets [4–6].

The τ phase is metastable and is formed in the miscibility gap between β-Mn (P4132, Mn *cP*20 type) and the intermetallic γ_2 (R3 m, Al_8Cr_5 type) by undercooling the high temperature hcp ε phase ($P6_3/mmc$, Mg type) [3]. Early investigations suggested that the ε → τ transformation is martensitic [7,8] but more recent studies established a massive transformation mode [9–11] with additional features of a displacive transformation [12]. The addition of C on interstitial lattice sites has been shown to hinder the decomposition of the τ phase, thus facilitating processing at elevated temperatures [13].

Hot extrusion of as-transformed τ-MnAl-C followed by an aging treatment was demonstrated, using an alloy of composition $Mn_{52.7}Al_{44.9}C_{2.4}$ (at.%), to yield a uniaxially textured bulk magnet with remanence of $\mu_0 M_r = 0.61$ T, coercivity of $\mu_0 H_c = 0.32$ T and energy density of $(BH)_{max} = 56$ kJ/m^3 [13]. These extrinsic magnetic properties are greatly improved compared to the as-transformed state [13] but further improvements, particularly in coercivity, are required in order to make MnAl-C magnets more attractive for applications. An increased coercivity of $\mu_0 H_c = 0.48$ T was demonstrated in mechanically milled MnAl powder [14] and even $\mu_0 H_c = 1$ T was achieved in MnAl thin films [15] and therefore it seems likely that higher coercivities in bulk materials are also possible. Coercivity is very sensitive to the microstructure [16] and improvements may be achieved if detailed knowledge of the microstructural features and their formation mechanisms during processing can be obtained and if the type of interaction of these features with magnetic domain walls can be ascertained. Processing routes can then be optimised to favour the formation of microstructural features which are beneficial for coercivity, for example.

Several studies using transmission electron microscopy (TEM) over the last decades have reported the presence of defects such as stacking faults, antiphase boundaries and twins in τ-MnAl and

* Corresponding author at: IFW Dresden, Institute for Metallic Materials, PO Box 270116, 01171 Dresden, Germany.
E-mail address: f.bittner@ifw-dresden.de (F. Bittner).

http://dx.doi.org/10.1016/j.actamat.2015.08.044
1359-6454/

MnAl-C [17–23]. The population of some defects is known to be sensitive to the sample state, for example antiphase boundaries were only observed in as-transformed samples but not after hot extrusion. In as-transformed samples, antiphase boundaries were reported to be often associated with magnetic domain walls [18–21] and therefore the higher coercivity of hot extruded samples has been partly attributed to the absence of antiphase boundaries [20,22]. Grain refinement, which occurs via dynamic recrystallization during hot extrusion [20,22], has also been reported to contribute to the increase in coercivity [20,24], possibly due to pinning of domain walls at grain boundaries [25]. Twins are common in both as-transformed and hot extruded conditions [18,20,21,23] and domain walls have been observed to be present at twin boundaries in both states [18,21,22]. From these results, an assessment of whether twin boundaries act as nucleation or pinning sites for magnetic domain walls cannot be made and therefore the effect of such boundaries on the coercivity is unclear.

The $L1_0$ structured γ-TiAl is analogous to τ-MnAl-C in that the parent phase has hexagonal symmetry in both cases. Three crystallographically different types of twin-like defects have been distinguished in γ-TiAl (c/a = 1.02 [26]) and the misorientation across the defect boundaries can be conveniently described by rotations of multiples of 60° about the normals to {1 1 1} planes [27,28] (see also Table 1). The $L1_0$ crystal structure can be described by two different unit cells: one contains 4 atoms (Pearson symbol *tP*4) and is related to fcc and the other contains 2 atoms (*tP*2) and is related to bcc. The lattice parameters of the two cells are related thus: $c_{tP2} = c_{tP4}$ and $a_{tP2} = \sqrt{2}\, a_{tP4}$. In this study the *tP*4 cell will be used. The existence of the three twin-like defects in $L1_0$ structured γ-TiAl can be attributed to two different twinning modes, which are similar to those found in the related fcc and bcc structures. Defects described by rotations of 60° or 180° about {1 1 1} derive from the fcc-based twinning mode $\langle 1\,1\,\bar{2}\rangle$ {1 1 1}, where the twinning plane is {1 1 1} and the shear direction is $\langle 1\,1\,\bar{2}\rangle$. The symmetry reduction of the $L1_0$ structure compared to fcc leads to a splitting of this twinning mode into two crystallographically different defects. Those described by a rotation of 180° about {1 1 1} are known as true twins and those described by a rotation of 60° about {1 1 1} are known as pseudo twins. The bcc-based twinning mode can be alternatively expressed using the *tP*4 cell as $\langle 1\,0\,1\rangle$ $\{1\,0\,\bar{1}\}$. This can be described by a rotation of 120° about {1 1 1} and such defects are referred to as order twins [29]. The order twins observed in γ-TiAl separated regions in which the *c*-axes were perpendicular to each other and the formation of these so-called *c*-domains was attributed to the accommodation of strain during the transformation from the hexagonal parent phase [28]. Such *c*-domains and the associated boundaries are also observed in systems where the parent phase is fcc [28,29].

To date only the existence of boundaries described by 180° rotations about {1 1 1}, *i.e.* true twins, has been shown in as-transformed and hot worked τ-MnAl using TEM [22,23]. The limitation of such high resolution studies is that only a relatively small area is available for analysis. Electron backscattered diffraction (EBSD) is an excellent alternative because it allows the investigation of much larger areas, albeit at a lower spatial resolution. In the current work, a detailed microstructural study of twin-like defects in MnAl-C samples in the as-transformed and hot extruded states has been carried out using EBSD for the first time. The aim of the work was to investigate whether all three twin-like defects are present in as-transformed and in subsequently hot extruded τ-MnAl-C and if so, whether the fractions of the three types are affected by the extrusion process. As the effect of twin boundaries on coercivity in MnAl-C is currently unknown, the results of this study will help to accelerate the development of MnAl-C magnets with improved properties.

Table 1
Summary of the 3 different twin-like defects in γ-TiAl $L1_0$ (c/a = 1.02 [26]), which are distinguished by rotations of multiples of 60° about the crystallographic {1 1 1} pole. Note that the twinning plane and shear direction of the order twin are given in *tP*4 notation.

Rotation angle about {1 1 1}	Denotation	Related twinning mode	Twinning plane	Shear direction
60°	Pseudo twin	fcc	{1 1 1}	$\langle 1\,\bar{2}\,1\rangle$
120°	Order twin	bcc	$\{1\,0\,\bar{1}\}$	$\langle 1\,0\,1\rangle$
180°	True twin	fcc	{1 1 1}	$\langle 1\,1\,\bar{2}\rangle$

2. Experimental procedure

An alloy with nominal composition $Mn_{53}Al_{45}C_2$ (at.%) was prepared by induction melting 99.99% pure Mn and Al with 99.9% pure C under argon atmosphere and was then cast in a cylindrical Cu mould of 10 mm diameter. The as-cast material was encapsulated in a glass tube which was evacuated to 10^{-4} mbar and then filled with 150 mbar of pure Ar. The tube was then placed into a furnace at 1100 °C and was left there for 2 days in order to homogenise the material. The tube was then removed from the furnace and quenched into water. Part of the homogenised material was hot extruded at 680 °C with an area reduction ratio of 4.

X-ray diffraction (XRD) was carried out using a Bruker diffractometer with Co-Kα radiation. The microstructure was studied using a Gemini Leo 1530 Scanning Electron microscope (SEM). The local crystallographic orientation was determined by electron backscattered diffraction (EBSD) measurements. An evenly spaced grid of measurement points with a spacing of 250 nm or 100 nm was chosen in the analysis region, yielding in total 40,000 data points for each measurement.

The magnetic properties were measured using a Quantum Design SQUID with applied fields up to 5 T at room temperature. The data were corrected for demagnetisation effects.

3. Results and discussion

3.1. General microstructure, texture and magnetic properties

The XRD pattern of the as-transformed sample is shown in Fig. 1. All reflexes can be attributed to τ. The inverse pole figure map of the as-transformed sample (Fig. 2a) is derived from EBSD data and shows the orientation of the sample normal direction with respect to the crystallographic directions. The as-transformed sample consisted of irregularly shaped grains of the τ phase, several tens of μm in size (Fig. 2a). In agreement with

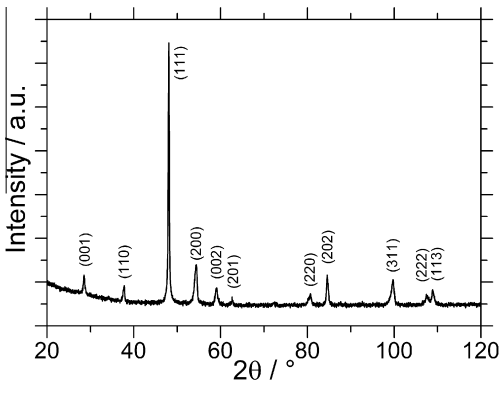

Fig. 1. XRD pattern of the as-transformed sample after quenching.

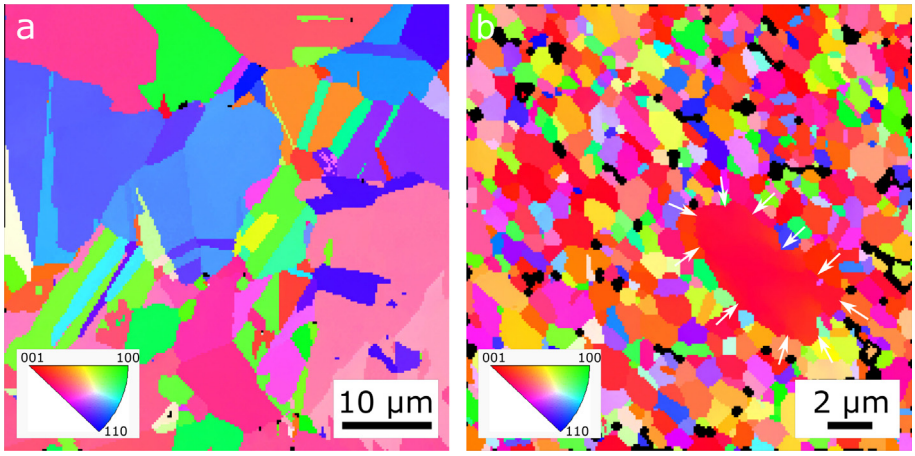

Fig. 2. Inverse pole figure maps derived from EBSD data: (a) as-transformed and (b) hot extruded (the white arrows mark large non-recrystallized grain). The colour of the grains represents the orientation of the sample normal with respect to the crystallographic poles. The colour code is given in the standard triangle shown in the inset. (For interpretation of the references to colour in this figure legend, the reader is referred to the web version of this article.)

the XRD results, no remnants of ε or other phases were observed by EBSD. One noticeable feature of the microstructure is the presence of a large number of planar interfaces, similar in appearance to twins (Fig. 2a).

The inverse pole figure map of the hot extruded material is shown in Fig. 2b. Hot extrusion led to a dramatic reduction of the average grain size to <1 μm (note that Fig. 2a and b have different scale bars). This grain refinement can be explained by the occurrence of dynamic recrystallization during the metal working at elevated temperatures [20,30]. Some larger non-recrystallized grains are still present, indicating that the microstructural reformation was not complete. These grains display a large twin density. One such polytwinned grain is marked by white arrows in Fig. 2b and a detailed view is shown in Fig. 3.

Some regions in the hot extruded material, especially the triple points between the τ grains could not be identified as τ and have therefore been coloured black in the orientation map (Fig. 2b). These regions correspond to other phases which were formed during hot extrusion and are likely to be either the equilibrium phases β-Mn and γ_2 [31] or the carbide, Mn_3AlC, which has been reported to be beneficial for coercivity [13,32].

The magnetic hysteresis loops of the material before and after hot extrusion are shown in Fig. 4a. The as-transformed sample (black line) shows a low coercivity of 20 mT. The magnetisation at an applied field of 2 T is 0.64 T but is still rising and reached a value of 0.78 T at an applied field of $\mu_0 H = 5$ T (data not shown).

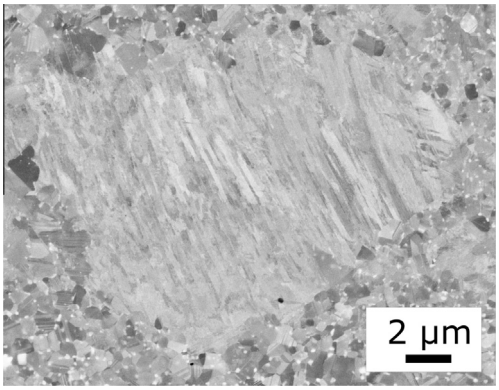

Fig. 3. Detailed view of a non-recrystallized grain which is surrounded by small dynamically recrystallized grains.

Hot extrusion changes the magnetic properties drastically. The remanence measured parallel and perpendicular to the extrusion direction is 0.47 T and 0.26 T, respectively. This anisotropy in the remanence was attributed to the formation of a crystallographic texture, in which the texture axis was parallel to the extrusion direction. The degree of texture (ω) can be estimated from the hysteresis loops as $\omega = (J_r^{\parallel} - J_r^{\perp})/J_r^{\parallel}$, where $J_r^{\parallel}$ and $J_r^{\perp}$ denote the remanence measured parallel and perpendicular to the texture axes, respectively. This value lies between 0 for non-textured (isotropic) and 1 for fully uniaxially textured samples. The calculated value of $\omega = 0.45$ corresponds to a medium texture.

A direct measurement of the texture was obtained from the EBSD data. Fig. 4b shows the inverse pole figure of the extrusion direction, which was determined from EBSD measurements over an area of 2500 μm^2 including more than 3000 recrystallized grains. The colour code corresponds to multiples of uniform pole density (M.U.D.). It can be seen that the intensity exhibits a maximum near the ⟨001⟩ direction, confirming the alignment of the magnetic easy axis of the grains (which corresponds to ⟨001⟩) in the extrusion direction. The intensity maximum at ⟨001⟩ is broad, indicating that the texture quality is medium. This is in good agreement with the result of the magnetic measurements.

The coercivity of the hot extruded sample increased to 0.16 T measured parallel to the texture axis and 0.20 T measured perpendicular to the texture axis. The increase in H_c is expected from the reduced grain size of the material but the possible contribution of special interfaces such as twins is currently unknown.

3.2. Twin-like defects

The crystallographic misorientation relating regions on either side of an interface can be expressed as a rotation about an axis common to both regions [33]. According to the tetragonal symmetry of the $L1_0$ crystal structure, 8 equivalent angle-axis pairs exist for each misorientation. The angle-axis pair with the smallest misorientation angle is known as the disorientation [34]. In order to investigate the presence of the three twin-like defect types, which can be described by rotations of multiples of 60° about {1 1 1}, in the as-transformed and extruded conditions, the following procedure was adopted. The disorientation between all pairs of neighbouring points in the EBSD data sets was calculated and all pairs where the disorientation angle was <5° were excluded from further analysis as these points were considered to be located inside the same subgrain. For all pairs of data points where the

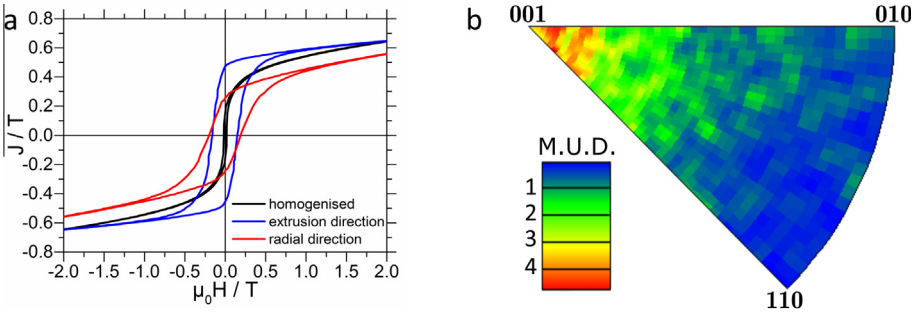

Fig. 4. Magnetic and crystallographic texture measurement of MnAl–C after hot extrusion: (a) magnetic hysteresis curve of the as-transformed (black line) and hot extruded sample measured parallel to the extrusion direction (blue line) and parallel to the radial direction (red line), (b) EBSD-derived inverse pole figure for the hot extruded sample showing the distribution of crystallographic poles parallel to the extrusion direction. (For interpretation of the references to colour in this figure legend, the reader is referred to the web version of this article.)

disorientation was >5°, each of the 8 equivalent angle-axis pairs was searched to find the one in which the misorientation axis was closest to a crystallographic {1 1 1} pole. The angle between the misorientation axis and the nearest {1 1 1} pole for all data points with disorientation >5° for the as-transformed and hot extruded samples is plotted in Fig. 5a and b. For the as-transformed state, the sharp maximum at low angles indicates that a large majority of the misorientation axes (81%) are within 2° of the nearest {1 1 1} pole and these misorientations can therefore be well described by a rotation about {1 1 1}. Misorientation axes with a larger angle to the nearest {1 1 1} pole appear only with a very low frequency. After hot extrusion, the peak at low angles is also present (Fig. 5b), indicating that misorientations which can be well described by rotations about {1 1 1} are very common. In addition, many data points where the angle between the misorientation axis and the nearest {1 1 1} pole are >2° appear, and these correspond to the large fraction of general grain boundaries visible in the EBSD data set for the extruded sample (Fig. 5b). For both samples, only

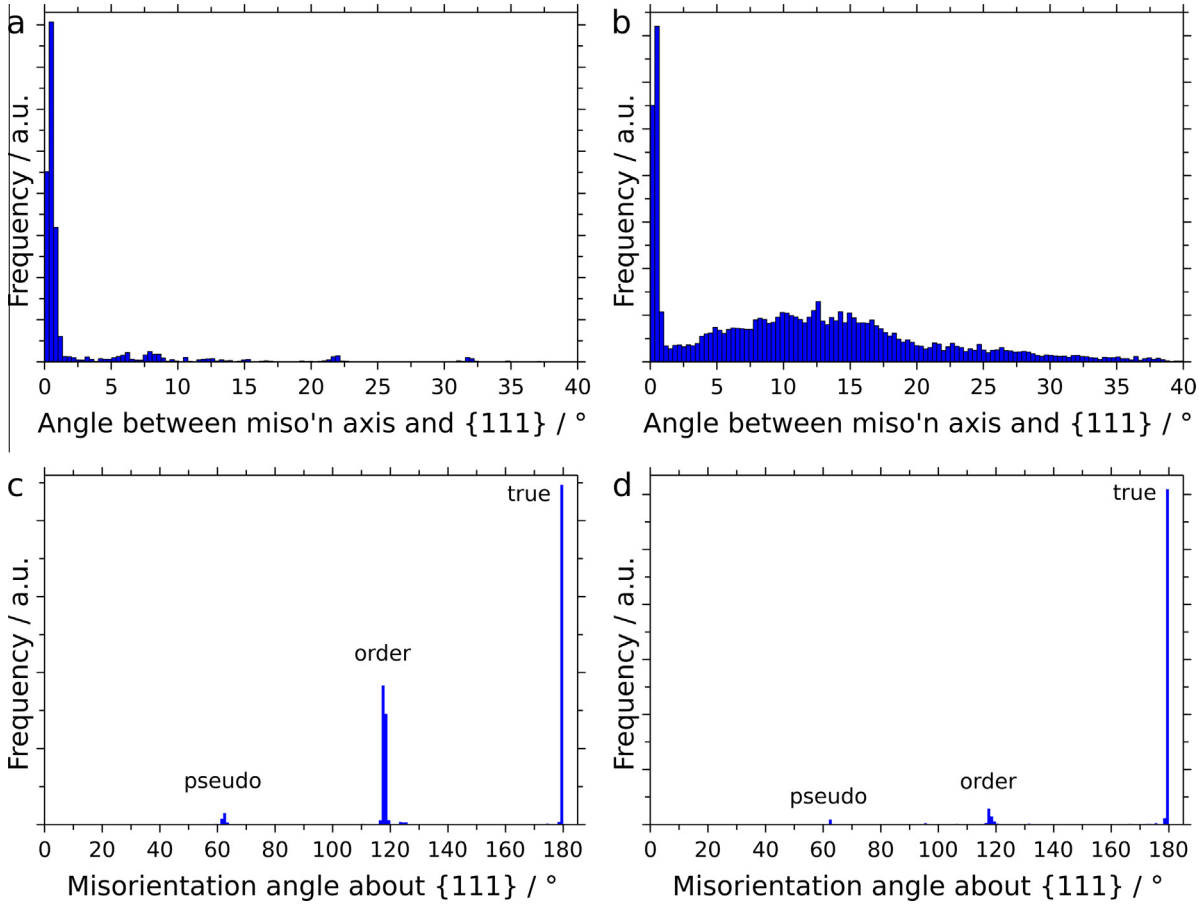

Fig. 5. Angle between the misorientation axis (miso'n axis) and the nearest {1 1 1} pole in (a) the as-transformed sample and (b) the hot extruded sample for all misorientations where the disorientation angle was >5°. Distribution of misorientation angles for all misorientations where the disorientation angle was >5° and the angle between the misorientation axis and the nearest {1 1 1} pole was <2° for (c) the as-transformed sample and (d) the hot extruded sample.

Table 2
Rotation angles about the normal of the {111} plane and fraction in as-transformed and hot extruded sample of the 3 different {111} related interfaces: pseudo twin, order twin and true twin.

Defect type	Rotation angle about {1 1 1}	Fraction in as-transformed sample	Fraction in hot extruded sample
Pseudo twin	62°	0.03	0.01
Order twin	118°	0.41	0.07
True twin	180°	0.54	0.84

misorientations where the angle between the misorientation axis and the nearest {1 1 1} pole was <2° were selected for further analysis.

The rotation angle distribution for all angle-axis pairs where the disorientation angle was >5° and the misorientation axis was within 2° of a {1 1 1} pole is shown in Fig. 5c and d for the as-transformed and hot extruded samples. In both samples 3 sharp maxima are visible and their positions are 62°, 118° and 180°. These measured rotation angles are not all exact multiples of 60°, as was the case for twin-like defects in γ-TiAl [28]. The lattice parameters of τ were determined by X-ray diffraction to be $a = 3.9156 \pm 0.0003$ and $c = 3.6257 \pm 0.0003$ Å, giving $c/a = 0.925$. This value is notably smaller compared to γ-TiAl and the different c/a ratio is responsible for the change of the misorientation angle [35]. Taking these small changes in the rotation angles into account, the measured rotation angle distributions show that all three twin-like defects introduced above (Table 1), pseudo twins, order twins and true twins, are present in $L1_0$ ordered τ-MnAl-C in both as-transformed and extruded conditions. In previous TEM studies of as-transformed samples only evidence of true twins was found [22,23] and the two other interfaces were not reported. That all three interfaces were found in the current work is likely to be because much larger areas were available for EBSD analysis and therefore the chance of finding all three interfaces was higher.

The three twin-like defects do not appear with the same frequency and their fractions for the different samples are shown in Table 2. Note that these are fractions of the total number of selected rotations about the {1 1 1} pole and not of the total amount of all interfaces in the sample. In the as-transformed sample, true twins show the highest content (54%), order twins account for 41% and pseudo twins for 3%. Hot extrusion leads to a remarkable change in the distribution of the different defect types: 84% of all detected {1 1 1} related misorientations are true twins, while the fraction of order twins and pseudo twins is reduced to 7% and 1%, respectively. In order to understand the change in the fractions of the various interfaces on hot extrusion, the formation mechanism of the interfaces must be considered.

The microstructure of the as-transformed sample originates directly from the ε → τ transformation. It is known from γ-TiAl, which undergoes a similar hexagonal → $L1_0$ transformation, that the order twins form due to strain which occurs during the transformation [28]. It is therefore very likely that the presence of the order twins in the as-transformed τ-MnAl-C sample is also attributed to transformation strains during the transformation from the hexagonal parent phase.

The spatial distribution of the three different interfaces is visualised in Fig. 6. Several triple points can be seen, where all 3 twin-like defects are found and one such configuration is marked by a white arrow in Fig. 6a. For cubic crystal structures, such triple points can be described by the simple rules proposed by Ranganathan [36]: if two interfaces meet at a triple point and they share a common rotation axis, then the sum of both misorientation angles gives the misorientation angle of the third interface, which must also share the same rotation axis. This rule can be applied to the present configuration pseudo twin–order twin–true twin. The local equilibrium can be expressed as 62°|{1 1 1} + 118°|{1 1 1} = 180°|{1 1 1}. From this result it can be concluded that if two of the three special interfaces interact at a triple point, the third one must necessarily be formed. In this way, the presence of the pseudo twins could be attributed to the interaction of true twins with order twins.

The microstructure of the hot extruded sample does not originate from the ε → τ transformation but rather from dynamic recrystallization of the deformed τ grains *i.e.* $\tau_{def} \rightarrow \tau_{rex}$. As the ε → τ transformation does not occur, the formation mechanism for the order twins does not exist and consequently the fraction of those interfaces is much lower in the extruded sample. The pseudo twins in the as-transformed sample were thought to form from the interaction of the true twins and order twins. As the fraction of order twins is much lower in the extruded sample, the chance of these interacting with true twins is much lower and as a result, the fraction of pseudo twins is lower than in the as-transformed sample. Both order twins and pseudo twins do appear after the dynamic recrystallization which occurred during extrusion, but with lower fractions than in the as-transformed state (Table 2, Fig. 6a and b). This is consistent with the interface distribution of recrystallized γ-TiAl, where a small number of pseudo

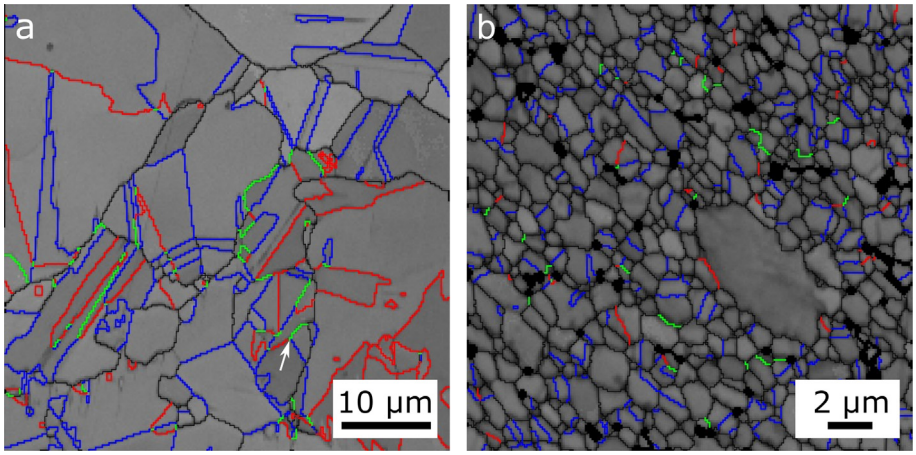

Fig. 6. Spatial distribution of the different {1 1 1} related interfaces in the different treated samples: (a) as-transformed and (b) hot extruded (The different coloured interfaces correspond to pseudo twins (green), order twins (red) and true twins (blue); other grain boundaries appear black). (For interpretation of the references to colour in this figure legend, the reader is referred to the web version of this article.)

and order twin boundaries were also observed, while the number of true twins was significantly higher [37].

3.3. Interaction with magnetic domain walls and interfacial structure of the twin-like defects

Having identified the three different twin-like defects in τ-MnAl-C and explained the change in the distribution of the boundaries after hot extrusion, the possible effect of the boundary types on the magnetic properties of the material must be considered. Since τ-MnAl-C is a uniaxial material, 180° domain walls are expected. The angle between the magnetically easy axis (parallel to ⟨001⟩) across the 3 different special interfaces is 48° for the pseudo twin, 75° for the true twin and 86° for order twins. As a consequence, it is possible that the three twin-like defects may interact differently with 180° domain walls. One important property determining this interaction is the nature of the interface. The special boundaries studied here are denoted as "twins" or "twin-like", because they fulfil the required misorientation relationship across the boundary. The twinning plane itself was not investigated in the present study, therefore no conclusions as to whether the interfaces are coherent can be given. If the boundary is planar and corresponds to the twinning plane (Table 1), it is expected that a coherent boundary would be formed. If the boundary plane does not correspond to the twinning plane, the presence of defects such as dislocations at the interface would be expected and these may also affect the passage of magnetic domain walls. In this case, the interface must not be necessarily planar. From Fig. 6 it can be seen that not all of the twin-like defects appear to be straight *i.e.* planar interfaces. It can therefore be concluded that incoherent interfaces are also present in both preparation conditions.

4. Conclusions

Twin-like defects have been studied using EBSD in $L1_0$ ordered τ-MnAl-C in the as-transformed and hot extruded states. Three crystallographically different twin-like defects, which can be described by rotation angles of 62°, 118° and 180° about {111}, appeared in both conditions. These were denoted as pseudo twins, order twins and true twins respectively. The small deviations in some of the measured rotation angles from multiples of 60° occurred because the c/a ratio of the $L1_0$ unit cell of the current materials was 0.925 instead of 1. This study gives the first evidence of the existence of pseudo twins and order twins in MnAl-C. By analogy with γ-TiAl, the order twins are considered very likely to form the boundaries between c-domains, which result from the accommodation of strains during the transformation from the parent ε phase to τ. The appearance of pseudo twins is symmetrically necessary when true and order twins interact and thus triple points with all three interfaces are observed.

The observed frequency of the three twin-like defects was very sensitive to the sample state. After hot extrusion and the associated dynamic recrystallization, the fraction of order twins and pseudo twins was strongly reduced. The high temperature phase ε is not involved in the dynamic recrystallization which occurs during hot extrusion and this reduces the content of order twins since their existence is directly connected to the ε → τ transformation. The reduced content of order twins led to a lower fraction of pseudo twins as fewer sites were present where true twins and order twins interacted. The misorientation angle between the magnetically easy ⟨001⟩ axes on either side of the three twin-like defects was 48°, 86° and 75° for pseudo twin, order twin and true twin respectively. The three interfaces may therefore have different interactions with 180° magnetic domain walls and may therefore have a different influence on the magnetic properties of the material. For a more profound understanding of the interaction of the three twin-like defects with magnetic domain walls, further investigations, including characterisation of the interfacial structure and modelling, are necessary.

Acknowledgements

The authors thank B. Gebel, H. Merker and M. Herrich for experimental assistance and Dr. K. H. Müller, T. Mix and R. Niemann for helpful discussions. The FP7 EU project ROMEO is kindly acknowledged for financial support.

References

[1] L. Pareti, F. Bolzoni, F. Leccabue, A.E. Ermakov, Magnetic anisotropy of MnAl and MnAlC permanent magnet materials, J. Appl. Phys. 59 (1986) 3824–3828.
[2] J.H. Park, Y.K. Hong, S. Bae, J.J. Lee, J. Jalli, G.S. Abo, et al., Saturation magnetization and crystalline anisotropy calculations for MnAl permanent magnet, J. Appl. Phys. 107 (2010) 09A731(3).
[3] H. Kono, On the ferromagnetic phase in manganese-aluminum system, J. Phys. Soc. Japan. 13 (1958) 1444–1451.
[4] J.M.D. Coey, Permanent magnets: plugging the gap, Scr. Mater. 67 (2012) 524–529.
[5] L.H. Lewis, F. Jiménez-Villacorta, Perspectives on permanent magnetic materials for energy conversion and power generation, Metall. Mater. Trans. A 44 (2012) 2–20.
[6] M.J. Kramer, R.W. McCallum, I.A. Anderson, S. Constantinides, Prospects for non rare earth permanent magnets for traction motors and generators, J. Miner. Met. Mater. Soc. 64 (2012) 752–763.
[7] S. Kojima, T. Ohtani, N. Kato, K. Kojima, Y. Salcamoto, I. Konno, et al., Crystal transformation and orientation of Mn–Al–C hard magnetic alloy, AIP Conf. Proc. 24 (1974) 768–769.
[8] J.J. van den Broek, H. Donkersloot, G. van Tendeloo, J. van Landuyt, Phase transformations in pure and carbon-doped Al45Mn55 alloys, Acta Metall. 27 (1979) 1497–1504.
[9] A.V. Dobromyslov, A.E. Ermakov, M.A. Uimin, Electron microscopy investigation of phase transformations in Mn–Al–C alloy, Phys. Status Solidi. 88 (1985) 443–454.
[10] D.P. Hoydick, E.J. Palmiere, W.A. Soffa, On the formation of the metastable $L1_0$ phase in manganese aluminum base permanent magnet materials, Scr. Mater. 36 (1997) 151–156.
[11] C. Yanar, J.M.K. Wiezorek, V. Radmilovic, W.A. Soffa, Massive transformation and the formation of the ferromagnetic $L1_0$ phase in manganese–aluminum-based alloys, Metall. Mater. Trans. A 33 (2002) 2413–2423.
[12] J.M.K. Wiezorek, A.K. Kulovits, C. Yanar, W.A. Soffa, Grain boundary mediated displacive-diffusional formation of τ-phase MnAl, Metall. Mater. Trans. A 42 (2010) 594–604.
[13] T. Ohtani, N. Kato, S. Kojima, K. Kojima, Y. Sakamoto, I. Konno, et al., Magnetic properties of Mn–Al–C permanent magnet alloys, IEEE Trans. Magn. 13 (1977) 1328–1330.
[14] Q. Zeng, I. Baker, J.B. Cui, Z.C. Yan, Structural and magnetic properties of nanostructured Mn–Al–C magnetic materials, J. Magn. Magn. Mater. 308 (2007) 214–226.
[15] S.H. Nie, L.J. Zhu, J. Lu, D. Pan, H.L. Wang, X.Z. Yu, et al., Perpendicularly magnetized τ-MnAl (001) thin films epitaxied on GaAs, Appl. Phys. Lett. 152405 (2013) 11–14.
[16] E.P. Wohlfarth, Hard magnetic materials, Adv. Phys. 8 (1959) 87–224.
[17] H. Zijlstra, H.B. Haanstra, Evidence by Lorentz microscopy for magnetically active stacking faults in MnAl alloy, J. Appl. Phys. 37 (1966) 2853–2856.
[18] J.P. Jakubovics, T.W. Jolly, The effect of crystal defects on the domain structure of Mn–Al alloys, Phys. B 86–88 (1977) 1357–1359.
[19] J.P. Jakubovics, A.J. Lapworth, T.W. Jolly, Electron microscope studies of ferromagnetic ordered structures, J. Appl. Phys. 49 (1978) 2002.
[20] J. van Landuyt, G. van Tendeloo, J.J. van den Broek, H. Donkersloot, H. Zijlstra, Defect structure and magnetic properties of MnAl permanent magnet materials, IEEE Trans. Magn. 14 (1978) 679–681.
[21] E.I. Houseman, J.P. Jakubovics, Domain structure and magnetization processes in MnAl and MnAlC alloys, J. Magn. Magn. Mater. 34 (1983) 1005–1006.
[22] E.I. Houseman, J.P. Jakubovics, Electron microscope study of the domain structure of MnAlC magnets, J. Magn. Magn. Mater. 31–34 (1983) 1007–1008.
[23] C. Yanar, V. Radmilovic, W.A. Soffa, M.K. Wiezorek, Evolution of microstructure and defect structure in $L1_0$ ordered manganese aluminide permanent magnet alloys, Intermetallics 9 (2001) 949–954.
[24] Z. Guang-qu, L. Shan-yi, W. Shao-jie, Investigation of microstructure and coercivity mechanisms in the permanent magnet alloy Mn–Al–C by positron annihilation and transmission electron microscopy, Phys. Status Solidi. 102 (1987) 165–169.
[25] J.D. Livingston, A review of coercivity mechanisms (invited), J. Appl. Phys. 52 (1981) 2544–2548.

[26] E.S. Bumps, H.D. Kessler, M. Hansen, Ti-Al system, Trans. Am. Inst. Minning Pet. Eng. 194 (1952) 609–614.
[27] C.R. Feng, D.J. Michel, C.R. Crowe, Twin relationships in TiAl, Scr. Metall. 22 (1988) 1481–1486.
[28] M. Yamaguchi, Y. Umakoshi, The deformation behaviour of intermetallic superlattice compounds, Prog. Mater Sci. 34 (1991) 1–148.
[29] D.W. Pashley, J.L. Robertson, M.J. Stowell, The deformation of CuAu I, Philos. Magn. 19 (1969) 83–98.
[30] O.A. Kaibyshev, R.Z. Valiev, A.K. Nurislamov, V.V. Stolyarov, Effect of the chemical composition on the structure and mechanical properties of alloys of the system Mn–Al–C in the magnetic region, Mater. Sci. Heat Treat. 30 (1989) 52–54.
[31] W.H. Dreizler, A. Menth, Transformation kinetics of the ferromagnetic alloy Mn–Al–C, IEEE Trans. Magn. 80 (1980) 534–536.
[32] C.T. Lee, K.H. Han, I.H. Kook, W.K. Choo, Phase and lattice parameter relationships in rapidly solidified and heat-treated (Mn0.53Al0.47)100 = xCx pseudo-binary alloys, J. Mater. Res. 7 (1992) 1690–1695.
[33] D.H. Warrington, P. Bufalini, The coincidence site lattice and grain boundaries, Scr. Metall. 5 (1971) 771–776.
[34] H. Mykura, Checklist of cubic coincidence site lattice relations, in: Grain Boundary Structure and Kinetics, ASM, Ohio, USA, 1980, pp. 445–456.
[35] A.H. King, A. Singh, Generalizing the coincidence site lattice model to non-cubic materials, J. Phys. Chem. Solids 55 (1994) 1023–1033.
[36] S. Ranganathan, On the geometry of coincidence-site lattices, Acta Crystallogr. 21 (1966) 197–199.
[37] V.Y. Gertsman, R.M. Gayanov, A.B. Notkin, R.Z. Valiev, Investigation of grain boundaries in TiAl intermetallic compound, Scr. Metall. Mater. 24 (1990) 1024–1032.